Self-consistent three-dimensional models for quantum ballistic transport in open systems

E. Polizzi
Laboratoire des Mathématiques pour l'Industrie et la Physique, Unité Mixte de Recherche CNRS 5640, Institut National des Sciences Appliqués, departement de Génie Mathématique et Modelisation, 135 Avenue de Rangueil, 31077 Toulouse Cedex 4, France

N. Ben Abdallah
Laboratoire des Mathématiques pour l'Industrie et la Physique, Unité Mixte de Recherche CNRS 5640, Institut National des Sciences Appliqués, departement de Génie Mathématique et Modelisation, 118 Route de Narbonne, 31062 Toulouse Cedex 4, France
(Received 12 November 2001; revised manuscript received 29 May 2002; published 4 December 2002)

A quasi-three-dimensional model for quantum ballistic transport in nanostructures is proposed. The model goes beyond the Thomas-Fermi approximation and is numerically more tractable than the full three-dimensional Schrödinger-Poisson model. Its derivation relies on the strong confinement of electrons at the heterojunction which allows us to split the three-dimensional Schrödinger equation into a one-dimensional Schrödinger equation for the confined direction and a two-dimensional Schrödinger equation in the transport direction. The space charge effects are taken into account in a three-dimensional framework. Numerical simulations of quantum waveguide devices such as T stubs and directional couplers are used to illustrate the accuracy of the quasi-3D model versus the fully 3D model and to show the importance of quantum effects.

DOI: 10.1103/PhysRevB.66.245301 PACS number(s): 75.40.Mg, 75.10.Jm, 02.70.−c

I. INTRODUCTION

Nanoscale split-gate devices such as quantum couplers, T stubs, etc., whose operation relies on the formation of a two-dimensional electron gas (2DEG) and on wave interference effects, have been widely studied both from the experimental and theoretical point of view.[1–12] At low temperatures, and thanks to the confinement of electrons in the 2DEG, the mobility is sufficiently high to consider the transport as ballistic along the 2DEG.[13–15] Therefore, the von Neumann or Schrödinger pictures are suitable. In the latter, electrons can be represented by a mixed state with given statistics, each elementary state being the solution of the Schrödinger equation with open boundary conditions.

Since the conductance is very sensitive to the value of the electrostatic potential, an accurate computation of space charge effects has to be done. For numerical reasons, the electrostatic potential used to be computed self-consistently in the Thomas-Fermi approximation.[9] Once the potential is obtained, the conductance is computed either by the Keldysh Green's functions[16–22] or mode matching techniques (the latter method requires the replacement of the potential by a hard wall potential).[23–26] The Thomas-Fermi approximation is only valid for equilibrium situations and for slowly varying electrostatic potentials. This is not the case for the devices we are interested in, as will be illustrated in the forthcoming sections. Therefore, an accurate representation of the electrostatic potential requires the resolution of the Schrödinger equations (thus allowing us to go beyond the Thomas-Fermi approximation). We shall perform this program by using the Lent and Kirkner boundary conditions[27] for each wave function [the quantum transmitting boundary method (QTBM), analogous results in electromagnetic were obtained in particular by Nedelec and Starling[28]]. Let us mention that the Schrödinger picture is suitable for ballistic transport since the density matrix is diagonal. When collisions are important, this approach is difficult to generalize (we, however, mention the Pauli master equation approach proposed by Fischetti in Ref. 29). The Keldysh Green's function approach is meeting an increasing interest since it allows us to easily take into account collisions. The idea consists in computing the density matrix directly by solving the Dyson equation, in which the collision can be incorporated in a rather direct way. The method is, however, very time consuming since off diagonal terms of the density matrix have to be computed. This results in doubling the number of position variables compared to the Schrödinger picture. In three-dimensional situations, this leads to a six-dimensional Dyson equation for which the numerical cost is high. Let us mention[21] where a new recursive Green's method is proposed for block diagonal Green's functions.

The method that we propose in this paper is based on the Schrödinger equation with the quantum transmitting boundary method. Numerical simulations in the two-dimensional case, without space charge effects, were performed in Ref. 30. In order to reduce the numerical complexity in the three-dimensional case, we propose a simplified quasi-three-dimensional model, which simultaneously takes into account the confinement of electrons in the 2DEG and the fact that the electrostatic potential is completely three-dimensional. This quasi-three-dimensional model is then compared with the fully three-dimensional one.

The outline of the paper is as follows. After having recalled the three-dimensional Schrödinger-Poisson system to be solved (Sec. II), we present in Sec. III the quasi-three-dimensional model. Section IV deals with the numerical procedure used to solve the defined coupled systems. The simulations of a T stub and a quantum directional coupler, presented in Sec. V, show a satisfactory agreement between the three-dimensional Schrödinger-Poisson model and the quasi-three-dimensional one (charge density, transmission spectra, etc), whose resolution requires much less computer resources. The comparison with classical models for charge density based on the three-dimensional and the two-

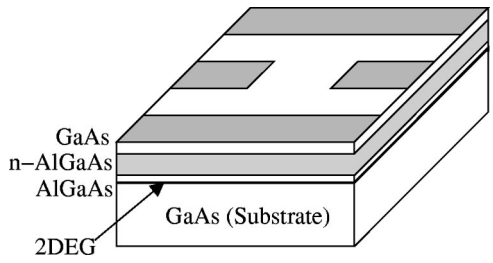

FIG. 1. Schematics of a quantum directional coupler. The device is composed by four semiconductor layers with Shottky gates on top.

dimensional Thomas-Fermi approximations shows that the Schrödinger approach is necessary to correctly model nanoscale split-gate devices.

II. THE THREE-DIMENSIONAL SCHRÖDINGER-POISSON SYSTEM

The structures that we are interested in are composed of an active region connected to reservoirs by quantum waveguides. Examples of such structures, and which we have simulated, are T stubs and directional quantum couplers which respectively contain two and four waveguides (see Fig. 1).

The three-dimensional domain (see Fig. 2) occupied by the device is a box denoted by Ω_0. We shall denote L_z its height and ω_0 its basis. The interface between the device and the waveguide number j is a rectangle denoted by Γ_j. We shall denote its horizontal side by γ_j

$$\Omega_0 = \omega_0 \times [0, L_z], \quad \Gamma_j = \gamma_j \times [0, L_z].$$

Since the system is open, the charge density correspond to the statistical mixture of scattering states

$$n(\vec{r}) = 2 \sum_{j_0, m_0} \int_0^\infty |\Psi_{j_0, m_0, k}(\vec{r})|^2 \times f_{\mathrm{FD}}\{E(j_0, m_0, k) - \mu_{j_0}\} \frac{dk}{2\pi}, \tag{1}$$

where the factor 2 is the spin factor, f_{FD} is the Fermi-Dirac distribution, and μ_{j_0} is the chemical potential associated to the waveguide j_0. The symbol $\vec{r} = (x, y, z)$ stands for the position variable. The wave function $\Psi_{j_0, m_0, k}$ corresponding to an incoming wave in the guide number j_0 on the transversal

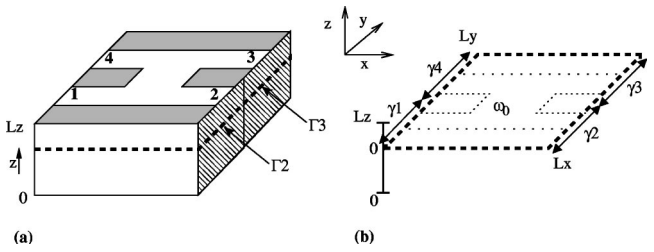

FIG. 2. Representation of the three-dimensional domain (active region Ω_0) with its boundaries (on the left) and its planar trace ω_0 (on the right).

mode m_0 (j_0 and m_0 are two integer indices), and with the wave vector k (k is a positive continuous index). These wave functions are scattering states of the Schrödinger Hamiltonian

$$H = -\frac{\hbar^2}{2m^*}\Delta + U(\vec{r}) \tag{2}$$

(U is the potential energy and m^* is the effective mass), and they are associated with the following energy:

$$E(j_0, m_0, k) = E_{m_0}^{j_0} + \frac{\hbar^2 k^2}{2m^*}, \tag{3}$$

where $E_{m_0}^{j_0}$ is the m_0th eigenvalue of the transverse Schrödinger equation in the guide j_0. We refer to Refs. 26 and 27 for a detailed description of suitable boundary conditions for these scattering states. The function $\Psi_{j_0, m_0, k}$ can be numerically computed by finite elements involving the QTBM.[27]

The potential energy U is defined by

$$U(\vec{r}) = -qV(\vec{r}) + E_c(z), \tag{4}$$

where E_c is the energy of the conduction band bottom, and $V(\vec{r})$ is the electrostatic potential. The electrostatic potential within the structure is self-consistently determined by solving the Poisson equation

$$-\nabla(\epsilon_r(z)\nabla V(\vec{r})) = \frac{q}{\epsilon_0}(\{n_D(z) - n[V](\vec{r})\}), \tag{5}$$

where q denotes the free electron charge, ϵ_0 the vacuum permittivity, ϵ_r the relative dielectric constant of the different semiconductors layers, and n_D the doping profile. The notation $n[V](\vec{r})$ expresses the fact that the density depends on the electrostatic potential V and stresses the nonlinear character of the problem. The boundary conditions used zero vertical electric field far inside the substrate ($z = 0$) because of charge neutrality, a given applied voltage at the top of the device ($z = L_z$) [the potential at the surfaces is assumed to be pinned at a fixed value $V_s = 0.7$ V (Refs. 31 and 32)] and is offset under the Shottky gates by the potential applied to the gates). Finally, zero longitudinal electric field is assumed on lateral faces because of the translation invariance of the potential in the waveguides. About the last point, we assume that the potential depends only on the transverse direction in the active region next to the Γ_j interface with the waveguide j. This means that the simulation domain has to be large enough to contain sufficiently long (but not too) portions of the waveguides.

III. THE QUASI-THREE-DIMENSIONAL SCHRÖDINGER-POISSON SYSTEM

We have solved the three-dimensional Schrödinger-Poisson system for the T stub and directional coupler situations, and obtained the self-consistent solution. This is described in Secs. IV and V. One of the major drawbacks of such resolution is its high numerical cost. We shall now

present a model that we call the quasi-three-dimensional model which takes into account the strong confinement of electrons in the z direction.

A. Description of the model

The 3D potential energy $U(\vec{r})$ can be separated arbitrarily into a potential U_1 depending on the vertical z direction, a potential U_2 depending on x,y, and a potential $u(\vec{r})$, such that

$$U(\vec{r}) = U_1(z) + U_2(x,y) + u(\vec{r}). \tag{6}$$

Let ϕ_n be the normalized eigenfunction solving the 1D eigenvalue problem

$$-\frac{\hbar^2}{2m^*}\frac{d^2}{dz^2}\phi_n(z) + U_1(z)\phi_n(z) = E_{zn}\phi_n(z), \tag{7}$$

with Dirichlet boundary conditions equal to zero at the top and the bottom of the device (respectively $z=0$ and $z=L_z$). The three-dimensional wave function Ψ_E can be expanded on the ϕ_n's

$$\Psi_E = \sum_{n=1}^{\infty} \psi^n(x,y)\phi_n(z), \tag{8}$$

In the particular case of $u=0$, the wave function ψ^n satisfies this 2D Schrödinger equation

$$-\frac{\hbar^2}{2m^*}\Delta_{x,y}\psi^n(x,y) + U_2(x,y)\psi^n(x,y) = (E - E_{zn})\psi^n(x,y). \tag{9}$$

In the general case, $u\neq 0$, the wave function ψ^n is then solution of the 2D Schrödinger equation (9) where the term $U_2\psi^n$ is replaced by

$$U_2(x,y)\psi^n(x,y) + \sum_{n'} \psi^{n'}(x,y)\left(\int_0^{L_z} \overline{\phi_n}(z)u(\vec{r})\phi_{n'}(z)dz \right), \tag{10}$$

and involves nondiagonal terms (those corresponding to $n' \neq n$).

The quasi-3D model consists in assuming that u is a slowly varying function compared to ϕ_n around the electron gas in the z direction, and neglecting the off-diagonal terms of Eq. (10). ψ^n is now the solution of a new 2D Schrödinger equation

$$-\frac{\hbar^2}{2m^*}\Delta_{x,y}\psi^n(x,y) + \hat{U}_n(x,y)\psi^n(x,y) = (E - E_{zn})\psi^n(x,y), \tag{11}$$

where the potential energy on the band number n is given by $\hat{U}_n(x,y) = U_2(x,y) + \int_0^{L_z} u(\vec{r})|\phi_n(z)|^2\, dz$, which can be rewritten

$$\hat{U}_n(x,y) = \int_0^{L_z} [U(\vec{r}) - U_1(z)]|\phi_n(z)|^2\, dz. \tag{12}$$

Let $\phi_{n_0}\psi^{n_0}_{j_0,p_0,k}$ be the wave function solving the quasi-3D problem and corresponding to one incoming wave in the waveguide j_0, on the vertical mode n_0, and the transverse mode p_0 in the guide. Therefore the energy is given by

$$E(j_0,p_0,n_0,k) = E_{zn_0} + \hat{E}^{j_0}_{p_0,n_0} + \frac{\hbar^2 k^2}{2m^*} \tag{13}$$

[where $\hat{E}^{j_0}_{p_0,n_0}$ is the p_0th eigenvalue of the 2D transverse Schrödinger equation (11) in the guide j_0] and the expression of the electron density takes now the following form:

$$n(\vec{r}) = \sum_{n_0=1}^{\infty} |\phi_{n_0}(z)|^2\, n^{n_0}_{2\mathrm{D}}(x,y), \tag{14}$$

where $n^{n_0}_{2\mathrm{D}}$ is defined as the 2D density of electrons in the vertical mode n_0

$$n^{n_0}_{2\mathrm{D}}(x,y) = 2\sum_{j_0,p_0} \int_0^{\infty} |\psi^{n_0}_{j_0,p_0,k}|^2 \times f_{\mathrm{FD}}\{E(j_0,p_0,n_0,k) - \mu_{j_0}\}\frac{dk}{2\pi}. \tag{15}$$

To summarize, the 3D wave function solution of Eq. (2) for a given energy can be separated in a 1D eigenvalue problem for the vertical z direction Eq. (7), and a two-dimensional Schrödinger equation (11) in the transport direction with open boundary conditions at the limit of the waveguides γ_j.

B. Approximation orders

Let the surface density and the current density be given by

$$ns(x,y) = \int_0^{L_z} n(\vec{r})dz \tag{16}$$

and

$$\mathbf{J}(\vec{r}) = 2\sum_{j_0,m_0} \int_0^{\infty} \mathbf{j}_{j_0,m_0,k}(\vec{r}) f_{\mathrm{FD}}(E(j_0,m_0,k) - \mu_{j_0})\frac{dk}{2\pi}, \tag{17}$$

where $\mathbf{j}_{j_0,m_0,k}(\vec{r})$ is the current density associated with one scattering state

$$\mathbf{j}_{j_0,m_0,k}(\vec{r}) = \frac{q\hbar}{m^*}\mathrm{Im}\{\overline{\Psi}_{j_0,m_0,k}(\vec{r})\nabla\Psi_{j_0,m_0,k}(\vec{r})\}. \tag{18}$$

We briefly summarize the results shown in Ref. 33. Assuming that $|u| \ll 1$, it can be shown using the stationary perturbation theory that the surface and the current intensities in the waveguides computed by the quasi-3D model are second order approximations of the corresponding quantities of the fully 3D model. The quasi-3D model is more accurate than the fully decoupled model (in which u is set to zero). Indeed, for the latter, the surface and current intensities in the waveguides are first order approximations of the correspond-

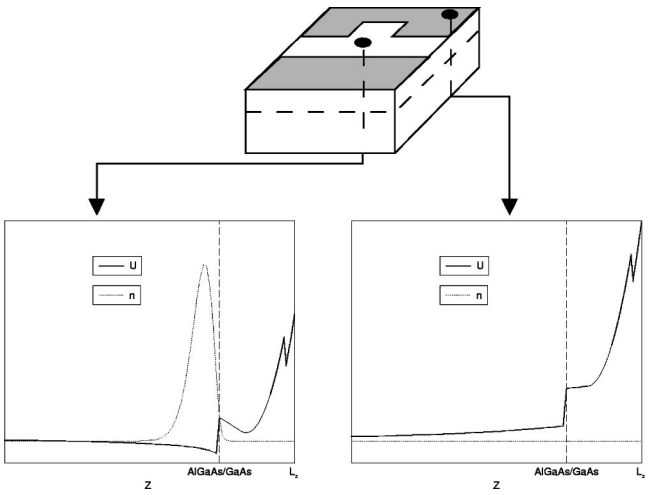

FIG. 3. Vertical potential and density profiles for a T stub at two different locations. In the active region (zone without gates on the top) the density is localized in the 2DEG next to the $Al_xGa_{1-x}As/GaAs$ interface, and in the zone under the gates, the electron density is equal to zero.

ing quantities of the fully 3D model. Moreover, the approximation orders are still valid if u is a slowly function compared to ϕ_n around the electron gas in the z direction (it is not necessary to have $|u| \ll 1$).

C. Description of the electron confinement through the quasi-3D model

For a given potential U, we need to define a potential U_1 which depends only on the z direction. When a negative bias potential is applied to the gates on the top of the device, the 2DEG deserts the zones under the gates in which the surface density is equal to zero. Figure 3 gives the potential and the density vertical profile for a zone under the gates and for the active region where are localized the electrons. The vertical potential U_1 is a potential which "must be seen" by the electrons. Therefore, we define the potential U_1 as a weighted average in the x,y direction of the 3D potential

$$U_1[V](z) = \frac{\int_{\omega_0} U(\vec{r}) ns[V](x,y)dxdy}{\int_{\omega_0} ns[V](x,y)dxdy}. \tag{19}$$

The chosen weight is the surfacic density in order to ignore the contributions of deserted zones; see Fig. 3. The quasi-3D quantum model is defined by the coupled system, Eqs. (16), (19), (7), (12), (15), (14), (4), and (5).

D. The current density

In this section we recall the expression of the current density in the waveguides using the transmission coefficients.[4,34]

In the 3D case and for one incoming wave in the input ports j_0 and the transverse mode m_0, the transmission coefficient in the output ports j and the transverse mode m is defined by

$$T_{j_0 \to j}^{m_0 \to m}(E) = \begin{cases} \dfrac{k_m^j(E)}{k_{m_0}^{j_0}(E)} |b_m^j|^2 & \text{if} \quad E \leqslant E_m^j \\ 0 & \text{else,} \end{cases} \tag{20}$$

The total transmission coefficient $T_{j_0 \to j}$ in the output ports j from the input port j_0 is given by

$$T_{j_0 \to j}(E) = \sum_{m_0,m} T_{j_0 \to j}^{m_0 \to m}(E). \tag{21}$$

In the quasi-3D case, the results about the transmission coefficient presented below are still valid with the following changes in expressions (20) and (21): The indices m_0 and m become, respectively, n_0, p_0 and n,p (the sums over the indices m_0 and m become, respectively, sums over the indices n_0, p_0 and n,p), and E_m^j becomes $\hat{E}_{p,n}^{j_0} + E_{zn}$.

Therefore, the electric current between the port j_0 and j is given by

$$I_{j_0 \to j} = \frac{q}{\pi\hbar} \int_0^\infty T_{j_0 \to j}(E) f_{\mathrm{FD}}(E - \mu_{j_0}) dE, \tag{22}$$

and the total current in the port j which takes into account the contribution of all port j_0 by

$$I_j = \sum_{j_0 \neq j} (I_{j_0 \to j} - I_{j \to j_0}). \tag{23}$$

We note $T_{j_0 \to j} = T_{j \to j_0}$ with the assumption of ballistic transport, and we obtain the following relation:

$$I_j = \frac{q}{\pi\hbar} \sum_{j_0} \int_0^\infty T_{j_0 \to j}(E)[f_{\mathrm{FD}}(E - \mu_{j_0}) - f_{\mathrm{FD}}(E - \mu_j)] dE. \tag{24}$$

At equilibrium, the chemical potentials are all equal to a single value μ. This implies with Eq. (24) that the currents are all equal to zero. Denoting v_j the applied bias at the port j, we obtain

TABLE I. Self-consistent 3D and quasi-3D models at equilibrium ($\mu_j = \mu$) and out of equilibrium.

	3D model	Quasi-3D model
$\mu_j = \mu$	Semiclassical Thomas-Fermi 3D Poisson 3D	Hybrid Schrödinger 1D Thomas-Fermi 2D Poisson 3D
$\mu_j = \mu - qv_j$	Quantum Schrödinger 3D Poisson 3D	Quantum Schrödinger 1D Schrödinger 2D Poisson 3D

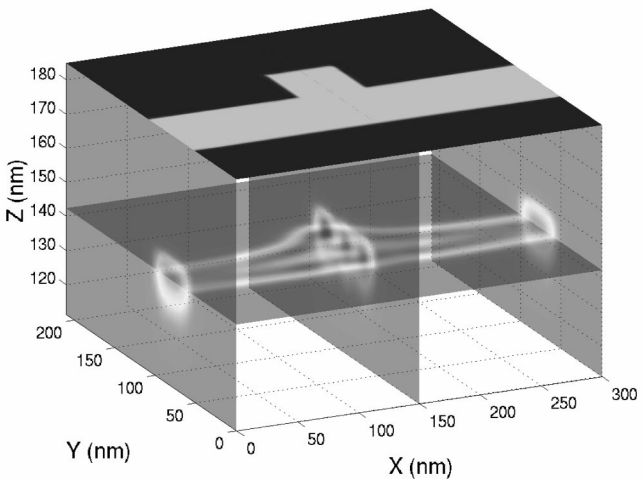

FIG. 4. The density profile after the quantum model convergence. Electrons are localized in the active region near the $Al_xGa_{1-x}As/GaAs$ interface.

$$\mu_j = \mu - q v_j , \tag{25}$$

and the net current is nonvanishing.

IV. NUMERICAL PROCEDURE

The P_1 finite element method is used to solve all the equations of the coupled systems on a same 3D mesh. It is convenient to construct the 3D mesh using parallel superposition of the same 2D mesh in the z direction since the quasi-3D models require a 1D mesh in the z direction to solve the vertical eigenproblem (7), and a 2D mesh on x,y to solve the 2D Schrödinger equation (11). The symmetric linear complex sparse systems that we obtain with the QTBM apply to the 2D or 3D open Schrödinger equations are solved using a quasiminimal residual (QMR) procedure.[35] In order to obtain the electron density for a given potential, we need to solve a large number of independent 2D or 3D open Schrödinger equations. Therefore, a parallel version of the code was developed.

Because of the highly nonlinear character of the coupled systems, implicit schemes have to be used for the numerical resolution. In order to obtain a suitable initial guess to begin the 3D and quasi-3D quantum simulations at equilibrium (with no applied bias voltage between the input and the output terminals of the structures), we use the well-known Thomas-Fermi semiclassical approximation. We briefly recall the expression of the electron density in this approximation

$$n[V(\vec{r})] = \frac{\sqrt{2}}{\pi^2}\left(\frac{m^*}{\beta\hbar^2}\right)^{3/2} F_{1/2}(\beta[\mu - U(\vec{r})]), \tag{26}$$

where μ is the chemical potential of the system at equilibrium, $\beta = 1/(k_B T)$, and $F_{1/2}(\eta_f)$ is the Fermi-Dirac integral given by

$$F_{1/2}(\eta_f) = \int_0^\infty \frac{\eta^{1/2}}{1+\exp(\eta - \eta_f)} d\eta. \tag{27}$$

The obtained 3D Thomas-Fermi/Poisson system is solved by standard Newton method. However, for the 3D quantum model and quasi-3D models the Newton method is not practical because the density depends non locally on the potential. Therefore, we use the Gummel iterations[36] and for a given potential V^n at the step n, the new potential V^{n+1} is now given by

$$-\nabla[(\epsilon_r(z)\nabla V^{n+1}(\vec{r})] + \frac{q}{\epsilon_0} n(\vec{r}) \frac{V^{n+1}}{V_{\text{ref}}} = \frac{q}{\epsilon_0}\left[n_D(z) - n(\vec{r})\left(1 - \frac{V^n}{V_{\text{ref}}}\right)\right], \tag{28}$$

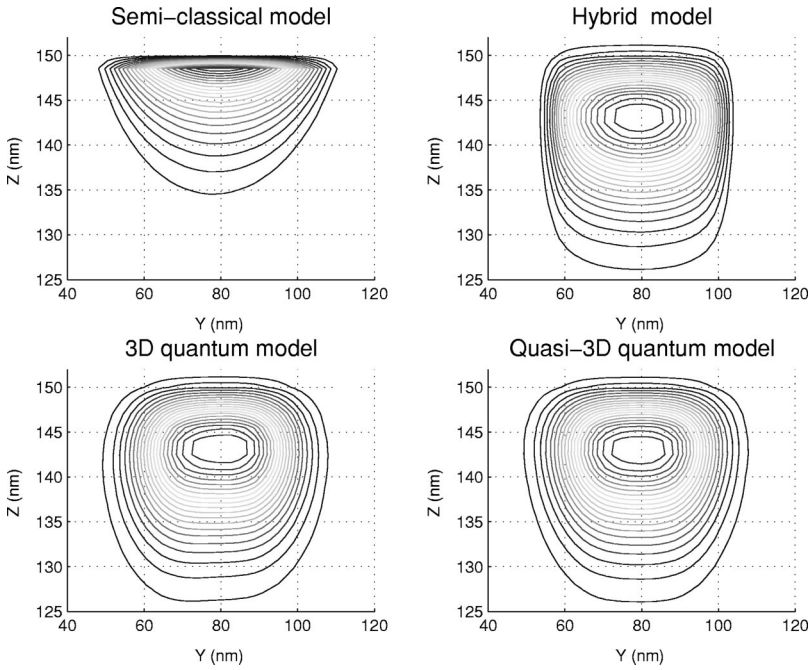

FIG. 5. Contour plots of the electron density in the waveguide $x=0$ far from the active region and for the four models at equilibrium.

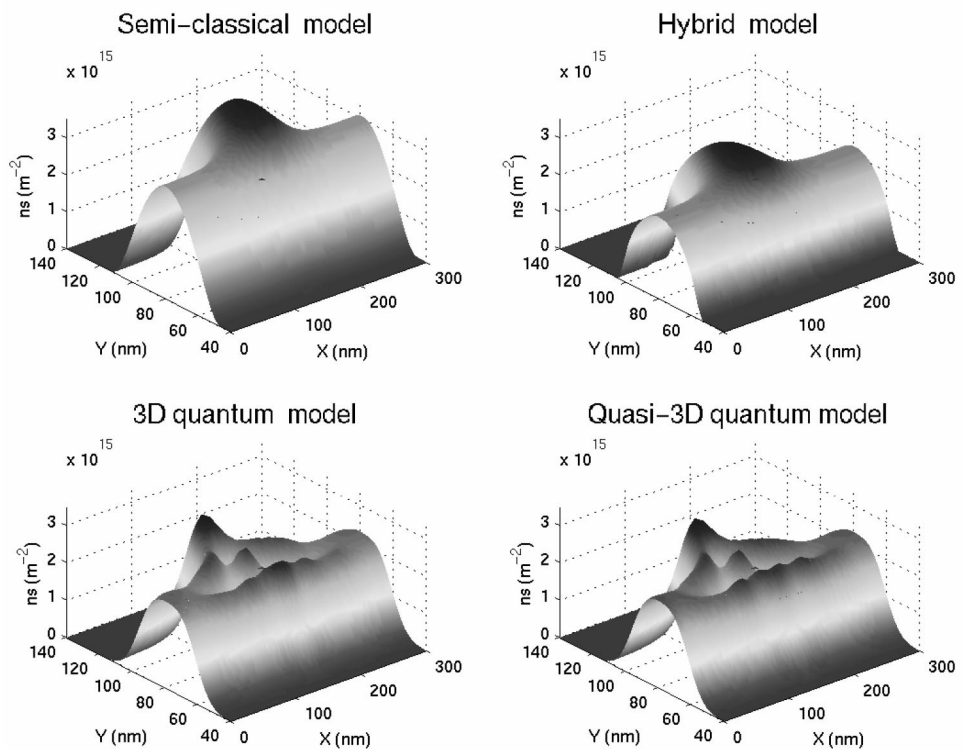

FIG. 6. The surfacic density profiles for the four models. In the quantum models, interference effects appear in the active region.

where V_{ref} is a reference potential (we choose $V_{\text{ref}} = k_B T/q$).

At equilibrium, we can also define a hybrid model which takes into account the quantum effect of the local constriction of electron gas in the z direction and consists in computing the 2D density of electrons defined in Eq. (14) by a semiclassical model. Therefore, the obtained potential of the hybrid coupled system is a better initial guess for both the 3D and quasi-3D quantum models at equilibrium. Table I summarizes the semiclassical and quantum models associated with the coupled systems that we have defined.

V. RESULTS

As an illustration of the models, we give some numerical results for the T stub and the quantum directional coupler. In our simulations, the dimensions of the three semiconductor layers between the gates and the substrate are successively 5,

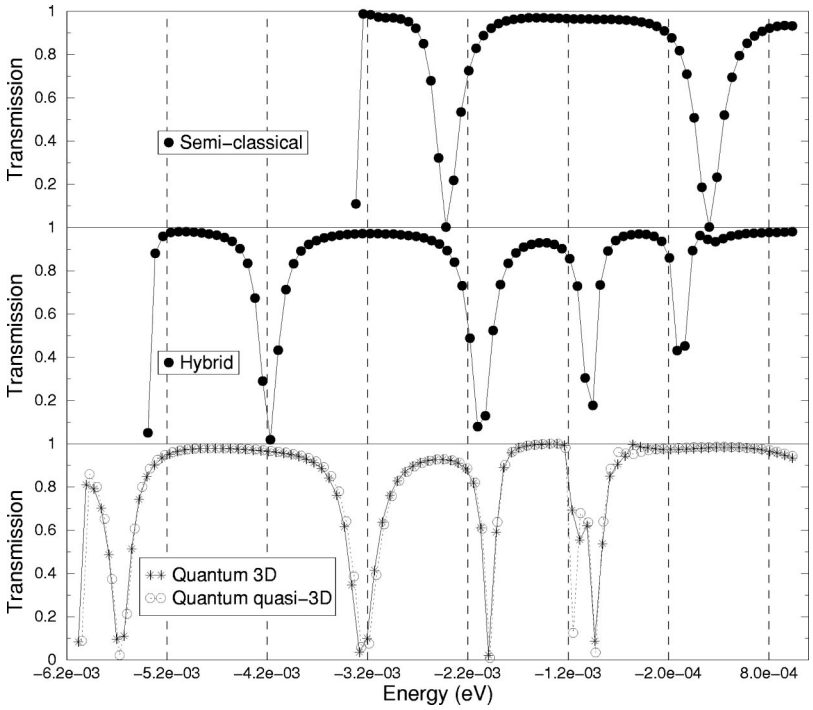

FIG. 7. Transmission coefficients for the four models. The results show a very good agreement between the 3D and quasi-3D models.

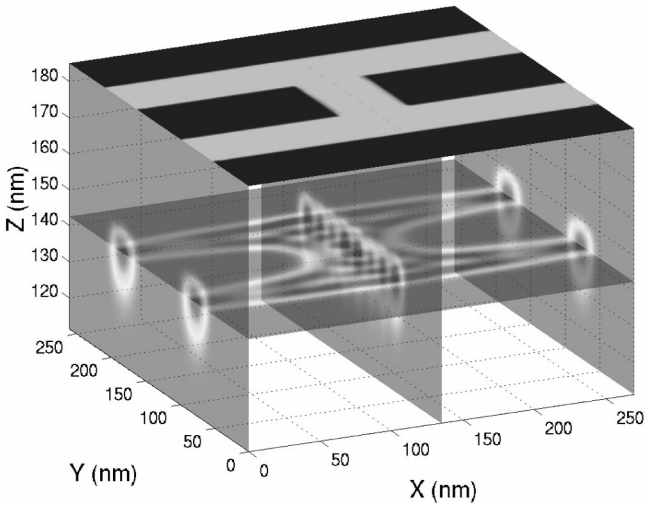

FIG. 8. The density profile after the quantum model convergence.

20, and 10 nm (we choose 150 nm for the substrate). We take an applied gates voltage equal to -0.5 V for the T stub and -0.53 V for the coupler, 4.2 K for the temperature, $n_D = 2.4\times 10^{18}$ cm^{-3} for the two first layers under the gates (the cap layer GaAs and n-$Al_xGa_{1-x}As$), $x=0.26$ for the portion of Al in $Al_xGa_{1-x}As$, $m^*=0.067m_e$ for the effective mass of GaAs (m_e is the electron mass), $\epsilon_r=12.88$ for the dielectric constant in all the device, $V_s=-0.7$ V for the pinning potential, and $\mu=0$ for the chemical potential at equilibrium ($v_1=v_2=0$ V). With these parameters, the electrons are localized in the first vertical mode $n=1$.

A. The T stub

The width of the waveguides on the top of the device is 60 nm, and the dimension of the cavity in the active region is 60×40 nm on x and y. We show in Fig. 4 the density profile in the device obtain with the quantum model where we denote the localization of the electron gas in a plane next to the $Al_xGa_{1-x}As$/GaAs interface (which is at $z=150$ nm) and only in the active region.

In Fig. 5, the electron density in the waveguides for the four models at equilibrium is given. In semiclassical simulations, the electron gas sits at the heterojunction while its mean position is 140.8 nm for the quantum model, almost 10 nm below the $Al_xGa_{1-x}As$/GaAs interface. In this latter, the electron gas appears more extended in the vertical direction. Moreover, there is a possibility for the electron to penetrate the heterojunction ($z>150$ nm) by tunneling effect (this result is still shown in Ref. 37 for the quantum wire case). The results on the density in the waveguides (far from the active region) obtained by the quasi-3D quantum model are very close to the results of the full 3D quantum model. This good agreement is also confirmed in the active region (see Fig. 6). Interference patterns appearing in the surfacic density computed by the quantum models and obviously absent for semiclassical simulations confirm the need for a quantum description.

More quantitatively, Fig. 7 shows the transmission coefficients for one incoming wave in the left waveguide ($x=0$) and in the first transverse mode. For all the models, the variations of the curves show oscillations between the total reflection (the transmission coefficient is equal to zero) and the total transmission (the transmission coefficient is equal to one). These kind of results were expected by the two-dimensional simulations with infinite wall potential and without space charge effects.[30] The transmission coefficients show a very good agreement between the 3D and quasi-3D models; this implies that the potential profile on the device is the same. The shift on the energy which appears between the semiclassical model and the others is due to vertical confinement of the electron gas and the fact that semiclassical model do not take it into account. Take note that the results given by the hybrid model (also for the surfacic density) are closer to the full quantum description than the results obtained by the semiclassical model.

The full 3D simulation requires huge computer resources. This is not true for the quasi-3D quantum model where the convergence speed is approximatively 215 time faster than the 3D model on a biprocesseur Compaq (DS20E). There-

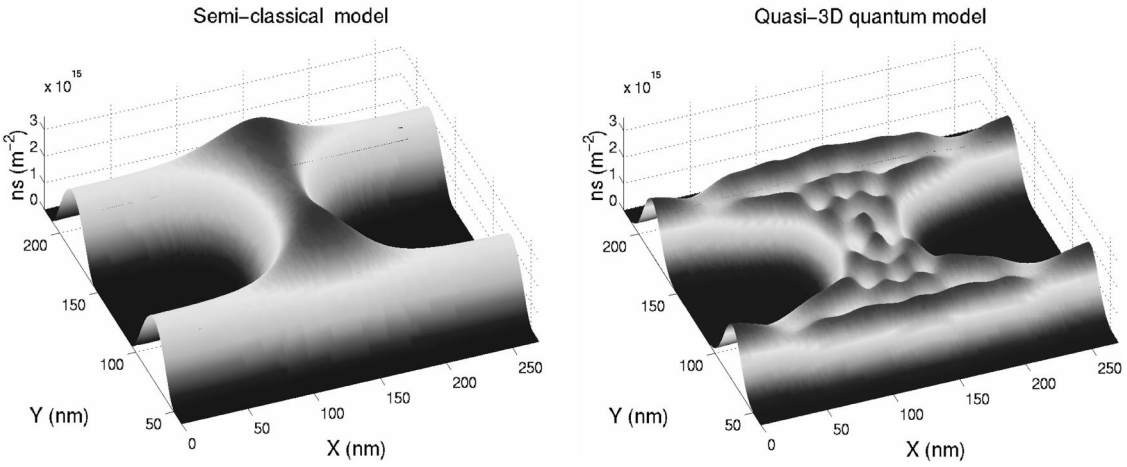

FIG. 9. The surfacic density profiles for the semiclassical model and the quasi-3D quantum model. In the quantum model, quantum effects appear in the active region.

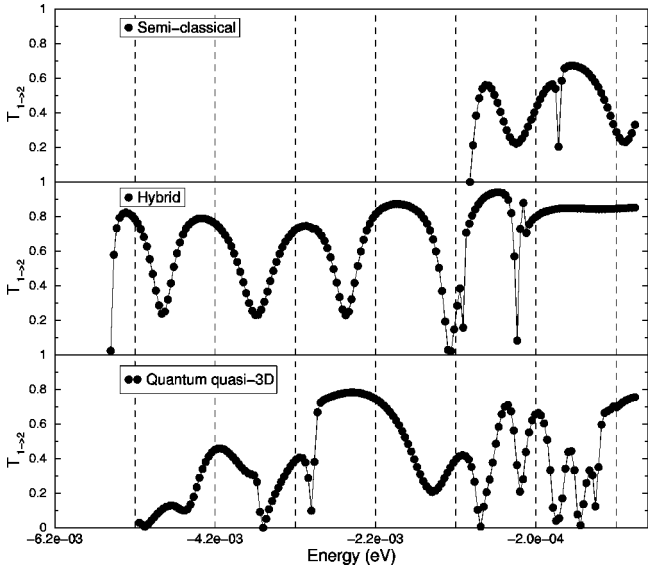

FIG. 10. Transmission coefficients in port 2 for one incoming wave in port 1 and for the three models.

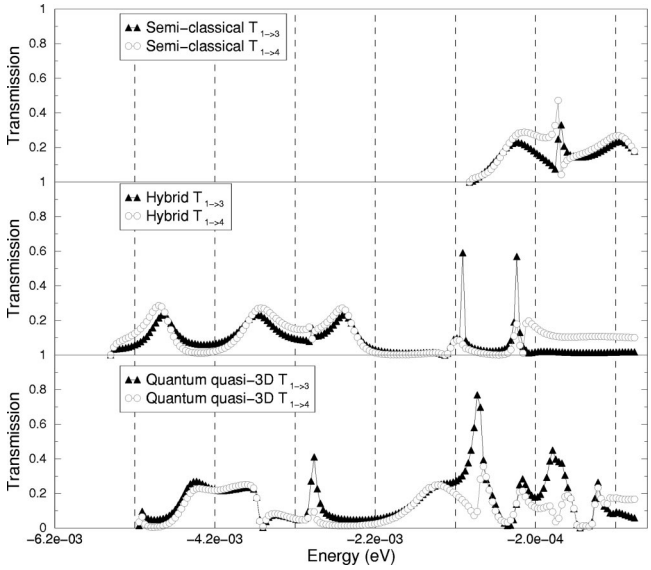

FIG. 11. Transmission coefficients in ports 3 and 4 for one incoming wave in port 1 and for the three models.

fore, the quasi-3D model can be used practically to compute current-voltage characteristics while it is quasi impossible for the 3D model.

B. The quantum directional coupler

The width of the waveguides on the top of the device is 50 nm, and the dimension of the coupling branch in the middle of the device is 50×60 nm on x and y. The geometry of the quantum directional coupler is more complex than the geometry of the T stub; then the number of the mesh nodes is also more important. The 3D quantum model in the quantum coupler case is then numerical expensive (the size of the linear systems obtained by solving the Schrödinger equations is too large to expect a result in relevant times). Therefore, we assume that the quasi-3D quantum model is a very good approximation of the full quantum model as it is shown for the T-stub case, and we only use this model for the quantum coupler simulations.

Figure 8 shows the density profile in the device obtained with the quasi-3D quantum model.

The mean position of the electron gas plane below the $Al_xGa_{1-x}As/GaAs$ interface is equal to 139.6 nm. The simulation exhibits very important quantum effects in the active region. This is not true for the semiclassical model, as shown in Fig. 9 for the surfacic density.

Figures 10 and 11 show the results of the transmission coefficients for one incoming wave in port 1 and in the first transverse mode, respectively, for a transmission in port 2, and transmissions in ports 3 and 4 (see Fig. 2 for the numbering of the ports).

The transmission coefficients obtained by the quantum model are very different from those obtained by the semiclassical or the hybrid one.

VI. CONCLUSION

To summarize, we have presented a Schrödinger-Poisson system modeling the electronic transport in a full 3D way and in a quasi-3D way. The latter can be derived from the full 3D model using a decomposition of the wave function which takes into account the vertical confinement of the electron in a 2DEG in the device. A very good agreement between the numerical results was obtained by the two models through the simulation of the T-stub device. The quasi-3D quantum model requires very small computer resources compared to the full 3D one. Moreover, we have shown a qualitative and quantitative comparisons, at equilibrium, between the quantum models and the semiclassical models based on the 2D and the 3D Thomas-Fermi approximations. These results confirm that a quantum description is required for complex devices such as the quantum directional coupler. In order to achieve the simulations, a 3D finite element code, called NESSIE (Nano-Electronic Simulator for System with Interference Effects) was developed at the MIP Laboratory. NESSIE is flexible enough to allow complex geometries which are defined by the gates on the top (with arbitrary numbers and directions for the waveguides) and so could be used to study a wide range of characteristics (current-voltage, temperature effects, conductance quantization effects, etc.) of many open quantum structures.

ACKNOWLEDGMENTS

We gratefully acknowledge helpful discussions with O. Vanbésien. This work benefited from the financial support of the TMR project, Contract No. ERB FMRX CT97 0157 as well as the CNRS project ''Transport dans les nanostructures'' (Action Spécifique STIC).

[1] See, for example, D.K. Ferry and S.M. Goodnick, Transport in Nanostructures (Cambridge University Press, Cambridge, 1997).
[2] N. Tsukada, A.D. Wieck, and K. Ploog, Appl. Phys. Lett. **56**, 2527 (1990).
[3] J. Wang, H. Guo, and R. Harris, Appl. Phys. Lett. **59**, 3075 (1991).
[4] M. Büttiker, Y. Imry, R. Landauer, and S. Pinhas, Phys. Rev. B **31**, 6207 (1985).
[5] J.O.J. Wesström, Appl. Phys. Lett. **82**, 2564 (1999).
[6] G. Xu, Y. Yang, and P. Jiang, J. Appl. Phys. **74**, 6747 (1993).
[7] O. Vanbésien and D. Lippens, Appl. Phys. Lett. **65**, 2439 (1994).
[8] F. Sols, M. Macucci, U. Ravaioli, and K. Hess, J. Appl. Phys. **66**, 3892 (1989).
[9] T. Palm, J. Appl. Phys. **74**, 3551 (1993).
[10] J.A. Del Alamo and C.C. Eugster, Appl. Phys. Lett. **51**, 78 (1990).
[11] P. Debray, O.E. Raichev, P. Vasilopoulos, M. Rahman, R. Perrin, and W.C. Mitchell, Phys. Rev. B **61**, 10 950 (2000).
[12] S. Datta, M.R. Melloch, S. Bandyopadhyay, and M.S. Lundstrom, Appl. Phys. Lett. **48**, 487 (1986).
[13] T. Ando, A.B. Fowler, and F. Stern, Rev. Mod. Phys. **54**, 437 (1982).
[14] J.J. Harris, C.T. Foxon, K.W.J. Barnham, D.E. Lacklison, J. Hewett, and C. White, J. Appl. Phys. **61**, 1219 (1986).
[15] L. Pfeiffer, K.W. West, H.L. Stormer, and K.W. Baldwin, Appl. Phys. Lett. **55**, 1888 (1989).
[16] G. Iannaccone, A. Trellakis, and U. Ravaioli, J. Appl. Phys. **84**, 5032 (1998).
[17] L.V. Keldysh, Zh. Éksp. Teor. Fiz. **47**, 1945 (1964) [Sov. Phys. JETP **20**, 1018 (1965)].
[18] M. Macucci, A. Galick, and U. Ravaioli, Phys. Rev. B **52**, 5210 (1995).
[19] H. Tsuchiya and T. Miyoshi, J. Appl. Phys. **83**, 2574 (1998).
[20] S. Sanvito, C.J. Lambert, J.H. Jefferson, and A.M. Bratkovsky, Phys. Rev. B **59**, 11 936 (1999).
[21] A. Svizhenko, M.P. Anantram, T.R. Govindan, B. Biegel, and R. Venugopal, J. Appl. Phys. **91**, 2343 (2002).
[22] J. Taylor, H. Guo, and J. Wang, Phys. Rev. B **63**, 245407 (2001).
[23] J.A. Nixon, J.H. Davies, and H.U. Baranger, Phys. Rev. B **43**, 12 638 (1991).
[24] A. Weisshaar, J. Lary, S.M. Goodnick, and V.K. Tripathi, J. Appl. Phys. **70**, 355 (1991).
[25] E. Tekman and S. Ciraci, Phys. Rev. B **39**, 8772 (1989).
[26] A. Szafer and A.D. Stone, Phys. Rev. Lett. **62**, 300 (1989).
[27] C.S. Lent and D.J. Kirkner, J. Appl. Phys. **67**, 6353 (1990).
[28] J.C. Nedelec and F. Starling, SIAM (Soc. Ind. Appl. Math.) J. Math. Anal. **22**, 1679 (1991).
[29] M.V. Fischetti, Phys. Rev. B **59**, 4901 (1999).
[30] E. Polizzi, N. Ben Abdallah, O. Vanbésien, and D. Lippens, J. Appl. Phys. **87**, 8700 (2000).
[31] J.H. Davies, Semicond. Sci. Technol. **3**, 995 (1988).
[32] M. Chen, W. Porod, and D.J. Kirkner, J. Appl. Phys. **75**, 2545 (1994).
[33] E. Polizzi, PhD. Thesis, INSA, Toulouse, France (2001).
[34] S. Datta and M.J. McLennan, Rep. Prog. Phys. **53**, 1003 (1990).
[35] R.W. Freund, SIAM (Soc. Ind. Appl. Math.) J. Sci. Stat. Comput. **12**, 425 (1992); **14**, 470 (1993).
[36] H.K. Gummel, IEEE Trans. Electron Devices **11**, 455 (1964).
[37] Z. Wu and P.P. Ruden, J. Appl. Phys. **74**, 6234 (1993).